Solid State Ionics 357 (2020) 115502

Contents lists available at ScienceDirect

Solid State Ionics

journal homepage: www.elsevier.com/locate/ssi

Surface analysis of lanthanum strontium cobalt oxides under cathodic polarization at high temperature through *operando* total-reflection X-ray absorption and X-ray fluorescence spectroscopy

Yoichiro Tsuji [a,b], Shinnosuke Sako [a], Kiyofumi Nitta [c], Kentaro Yamamoto [a], Yang Shao-horn [d], Yoshiharu Uchimoto [a], Yuki Orikasa [e,*]

[a] Graduate School of Human and Environmental Studies, Kyoto University, Yoshida-nihonmatsucho, Sakyo-ku, Kyoto 606-8501, Japan
[b] Technology Division, Panasonic Corporation, 3-1-1 Yagumo-naka-machi, Moriguchi City, Osaka 570-8501, Japan
[c] Japan Synchrotron Radiation Research Institute, 1-1-1 Kouto, Sayo-cho, Hyogo 679-5198, Japan
[d] Department of Mechanical Engineering, Massachusetts Institute of Technology, 77 Massachusetts Avenue, Cambridge, MA 02139, United States
[e] Department of Applied Chemistry, College of Life Sciences, Ritsumeikan University, 1-1-1 Noji Higashi, Kusatsu, Shiga 525-8577, Japan

ARTICLE INFO

Keywords:
Solid oxide fuel cell
Cathode
Operando X-ray absorption spectroscopy
Sr segregation

ABSTRACT

The surface chemistry of perovskite-type lanthanum transition metal oxides is an important parameter in high-temperature electrochemical devices such as solid oxide fuel cells (SOFCs). Strontium segregation on the surface of lanthanum strontium cobalt oxides (LSC) may lead to poor oxygen reduction kinetics. However, previous studies have not sufficiently addressed the oxide surface chemistry, including the oxidation change of LSC under cathodic polarization. In this study, *operando* total-reflection X-ray fluorescence absorption and X-ray fluorescence spectroscopy were performed to investigate cathodic polarization at high temperature (773 K) and at 1 atm pressure. Dense thin-film electrodes of $La_{0.6}Sr_{0.4}CoO_3$ (LSC_{113}) on $Zr_{0.92}Y_{0.08}O_{1.96}$ electrolytes with a gadolinium-doped ceria interlayer were examined as model SOFC cathodes. This may be the first time that predominant surface reduction of cobalt is directly observed by using LSC_{113} under cathodic polarization. This phenomenon is related to strontium enrichment on the LSC surface. $(La_{0.5}Sr_{0.5})_2CoO_4$ decoration on LSC_{113} enhanced the oxygen reduction kinetics compared with that of bare LSC_{113}. This is due to the suppression of cobalt surface reduction and Sr enrichment in the LSC_{113} phase.

1. Introduction

Reducing the operating temperature of solid oxide fuel cells (SOFCs) is advantageous because it reduces the cell operating cost and improves durability, which can broaden the practical applications of SOFCs [1]. However, kinetics of the cathode reaction considering the conversion of the oxygen gas to the oxide ion, and the subsequent ion transport into the electrolyte, is diminished at low temperature [2]. In order to enhance cathode kinetics, the cathode reaction mechanism at high temperature must be elucidated. Oxygen reduction on the electrode surface is one of the primary reactions that occur in the SOFC cathodes [3]. For cathode reactions using typical perovskite or Ruddlesden–Popper oxide cathodes, except for lanthanum manganese oxides, oxygen reduction including adsorption and ionization is the rate-limiting step [4–8]. The importance of cathode surface reactions in SOFCs motivated us to investigate the surface chemistry of cathode materials. Because such surface phenomena are considered to be specific under high temperature conditions, *in situ* or *operando* observation of the nanosurface can lead to a novel approach for understanding cathode reactions [9].

$La_{1-x}Sr_xCoO_{3-\delta}$ and their related perovskite oxides are representative cathode materials and have been considered as potential cathode materials for SOFCs because of their high ionic and electric conductivity properties [10,11]. Previous studies related to the surface analysis of perovskite oxides have identified the formation of a Sr-enriched phase (*i.e.*, Sr segregation) at high temperature [12–23], which induces compositional changes in cathode materials and impedes the kinetics of cathode reactions. During SOFC operation, the cathodic polarization of the electrodes also influences the surface chemistry. Sr segregation reduction is an efficient path to enhance the surface cathode reactions.

* Corresponding author.
E-mail address: orikasa@fc.ritsumei.ac.jp (Y. Orikasa).

https://doi.org/10.1016/j.ssi.2020.115502
Received 11 September 2020; Received in revised form 12 October 2020; Accepted 19 October 2020
Available online 29 October 2020

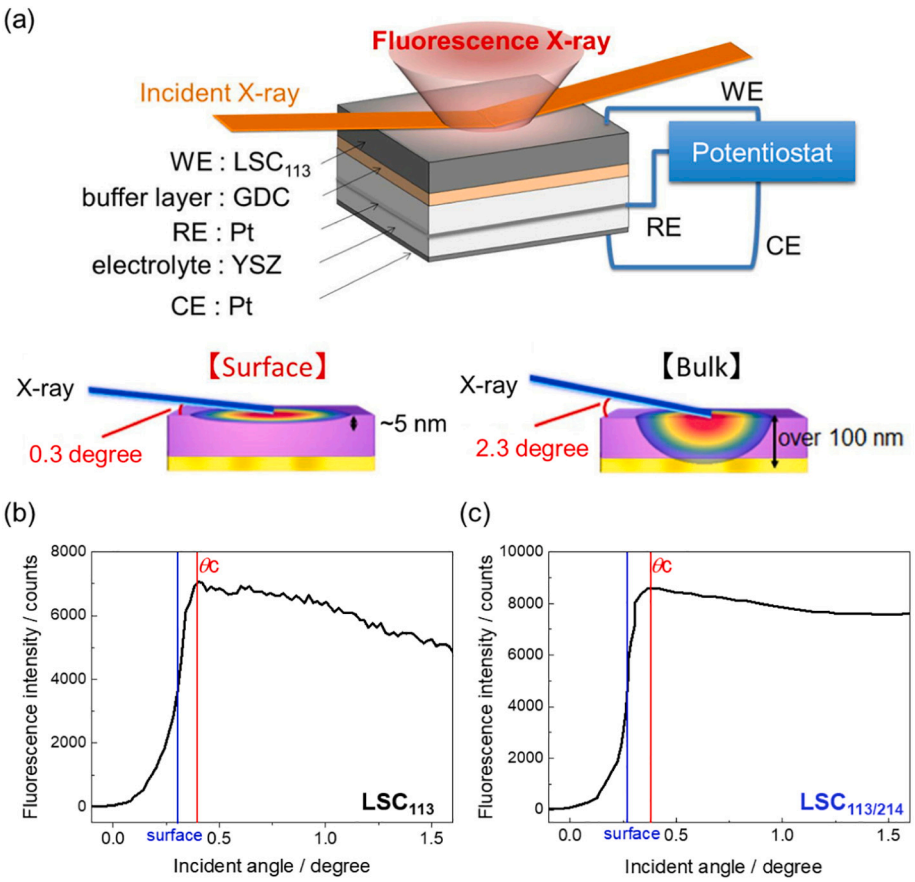

Fig. 1. (a) Schematic of the setup for data collection in the *operando* total-reflection XAS cell. Fluorescence counts as a function of incident angle of (b) LSC_{113} and (c) $LSC_{113/214}$. The penetration depth was denoted as "surface"(blue font). (For interpretation of the references to colour in this figure legend, the reader is referred to the web version of this article.)

Since the enhanced oxygen exchange reaction at the heterostructured oxide interface between $La_{1-x}Sr_xCoO_{3-\delta}$ and $La_{2-x}Sr_xCoO_{4\pm\delta}$ was found [24], the improved kinetics of the cathode reaction using $La_{1-x}Sr_xCoO_{3-\delta}$–$La_{2-x}Sr_xCoO_{4\pm\delta}$ mixed composite perovskite [25,26], $La_{1-x}Sr_xCoO_{3-\delta}$ thin films decorated with strontium oxide, and $La_{2-x}Sr_xCoO_{4\pm\delta}$ have been reported [12–15,27]. Studies based on the thin-film interface model between $La_{1-x}Sr_xCoO_{3-\delta}$ and $La_{2-x}Sr_xCoO_{4\pm\delta}$ have reported the presence of a stable phase of $La_{2-x}Sr_xCoO_{4\pm\delta}$ on the surface at high temperature and the observation of a large number of active sites for oxygen dissociation–incorporation under cathodic polarization [19]. These surface mechanisms are commonly explained by X-ray photoemission spectroscopy, because it is a surface-sensitive analytical technique. Considering the oxygen potential profile under cathodic polarization at high temperature [4], the oxygen non-stoichiometry and oxidation state of cations in the electrode bulk change significantly [28], which is considered to influence the electrode surface. Moreover, the chemical analysis of cations combined with surface analysis can elucidate the mechanism of the oxygen reduction reaction (ORR) at high temperature.

To determine the oxidation state of transition metals, X-ray absorption spectroscopy (XAS) is an effective technique that provides information on the electronic and local structures of absorbance atoms [9]. It is possible to analyze the chemical state of target atoms, because XAS data are related to specific atoms. In addition, spectra in the hard X-ray region can be obtained even in the presence of oxygen gas. Therefore, XAS has been used for *in situ* analysis of SOFC cathodes under high temperature and pressure conditions [6,7,29–35]. Although standard XAS reflects bulk information, the use of geometry setups including grazing incident X-ray diffraction [36] or low-angle X-ray fluorescence [37,38] can provide surface-sensitive spectra. We have previously detected oxidation changes related to the surface segregation phenomena of $La_{0.8}Sr_{0.2}CoO_3$ thin films at high temperature by depth-resolved XAS [39].

In this study, the surface oxidation state of transition metals in lanthanum strontium cobalt oxides (LSC) was determined during cathodic polarization and compared with that of the bulk state. $La_{0.6}Sr_{0.4}CoO_{3-\delta}$ thin-film electrodes on yttrium-stabilized zirconium (YSZ)-poly crystalline substrates with a gadolinium-doped ceria interlayer were prepared by pulse laser deposition (PLD), followed by decoration with $(La_{0.5}Sr_{0.5})_2CoO_{4\pm\delta}$ of various thicknesses. Oxygen reduction kinetics for the electrodes were examined by electrochemical polarization and impedance measurements. The surface oxidation state was analyzed using *operando* total-reflection fluorescence X-ray absorption spectroscopy (TRF-XAS), which integrates the fluorescence yield obtained under total reflection and allows the investigation of surface reactions at the nanoscale under cathodic polarization. Furthermore, by conducting *operando* (TRF-XAS)-based XRF analysis, elemental analysis of LSC was performed under the operating conditions. Through the combination of these techniques, the electronic structure and elemental content change that occurred on the electrode surface of the LSC thin-film electrode were determined.

2. Experimental

2.1. Sample preparation

LSC [$La_{0.6}Sr_{0.4}CoO_{3-\delta}$ and $(La_{0.5}Sr_{0.5})_2CoO_{4\pm\delta}$] thin films (the oxides are defined as LSC_{113} and LSC_{214}, respectively) were prepared by PLD

with a YAG laser (λ = 256 nm). The target samples were synthesized through a conventional solid-state reaction and a complex polymerization process. To prepare LSC_{113}, stoichiometric amounts of La_2O_3, CoO, and $Sr(NO_3)_2$ (Wako Pure Chemical) were mixed in a mortar. Subsequently, calcination was performed at 1423 K for 5 h. The resulting LSC_{113} powder was pressed into pellets and sintered at 1523 K for 10 h under air. To prepare LSC_{214}, La_2O_3 (Kojundo Chemical) was pre-dried at 1273 K under air and dissolved in nitric acid. Then, stoichiometric amounts of $Co(NO_3)_2{\cdot}6H_2O$ and $Sr(NO_3)_2$ (Wako Pure Chemical) were added until dissolved. Citric acid and ethylene glycol were added in excess to the solution. The solution was gradually fired at 423 K to obtain a gel. Organic residuals were removed by heating at 673 K, and this precursor was calcined at 1273 K for 10 h. Gadolinium-doped ceria (GDC, Rhodia, Japan) was used as the buffer layer. GDC powder was pressed into pellets and sintered at 1473 K for 10 h under air. Separately, YSZ powder was pressed into pellets and sintered at 1773 K for 10 h under air. The sintered YSZ pellets were mirror-polished and used as the substrate; the base pressure in the chamber was $<10^{-5}$ Pa. Deposition under 10 Hz repetition was performed for 5 min using a GDC target and for 15 min for the LSC_{113} thin film at a substrate temperature of 1173 K. Decorated deposition of LSC_{214} was performed on LSC_{113} through numerous pulses (25–2700 pulses) at a substrate temperature of 1173 K. All film samples were characterized by X-ray diffraction (XRD, Rigaku RINT2200) with Cu-K_α (40 kV, 40 mA). To perform *operando* TRF-XAS and XRF, an (110)-oriented YSZ single crystal was used as a substrate for PLD because a thin film sample with a flat and smooth surface was required. The PLD preparation conditions were similar for each thin film when using a polycrystalline YSZ substrate, and the LSC_{214} thin film obtained with 900 pulses was selected because it showed the highest ORR activity. The thin films prepared on (110)-oriented YSZ single-crystal substrates were characterized by XRD, atomic force microscopy (AFM), and transmission electron microscopy (TEM).

2.2. Electrochemical testing

A three-electrode cell was constructed to determine the electrochemical performance (Fig. S1) at 1073 K and under the open circuit condition (OCV) at oxygen partial pressure [$p(O_2)$] of 10^5 Pa. The working electrode (WE) consisted of LSC_{113} decorated with LSC_{214}. The counter electrode (CE) and reference electrode were porous platinum. Electrochemical impedance spectroscopy (EIS) data and direct current (DC) polarization of the film electrodes were respectively conducted using an impedance analyzer and a potentiostat (Solartron 1255 and 1287, respectively). Impedance measurements were conducted over the frequency range from 1 MHz to 0.1 Hz with an amplitude alternating current voltage of 10 mV.

2.3. Operando XAS and XRF analysis

A three-electrode cell using thin films was prepared to perform *operando* TRF-XAS and XRF at the BL01B1 beamline (SPring-8, JASRI, Japan). Co *K*-edge X-ray absorption near-edge spectroscopy (XANES) was conducted under the fluorescence mode using a 19-element Ge solid-state detector (SSD). A schematic of the TRF-XAS setup of the cell is shown in Fig. 1a. XAS and XRF measurements were performed at 773 K and $p(O_2)$ of 10^5 Pa under OCV. In addition, the measurements under constant polarizations of −100 and − 900 mV (WE–CE) were conducted. Figs. 1b and c show the fluorescence detector counts as a function of the incident angle for LSC_{113} and LSC_{113} with 3 nm of LSC_{214} decoration (denoted as $LSC_{113/214}$). The calculated critical angle of total reflection (θ_c) for LSC_{113} was 0.375°. The highest count was observed at 0.40° and 0.38° for LSC_{113} and $LSC_{113/214}$, respectively, which was consistent with the calculated angle. Because the incident angle for the surface region of the sample was required to be smaller than θ_c, we set half of the SSD counts of the highest counts as the surface measurement angle. When the incident angle was set at 0.30°, the penetration depth was estimated to be ~5 nm (denoted as "surface" in Figs. 1b and c). The bulk information was obtained by setting the incident angle at 2.3°; under that condition, the penetration depth was estimated to be >100 nm. Considering that the thickness of LSC_{113} was ~60 nm, information regarding this film could be obtained. XRF spectra were also collected at an incident energy of 16.5 eV.

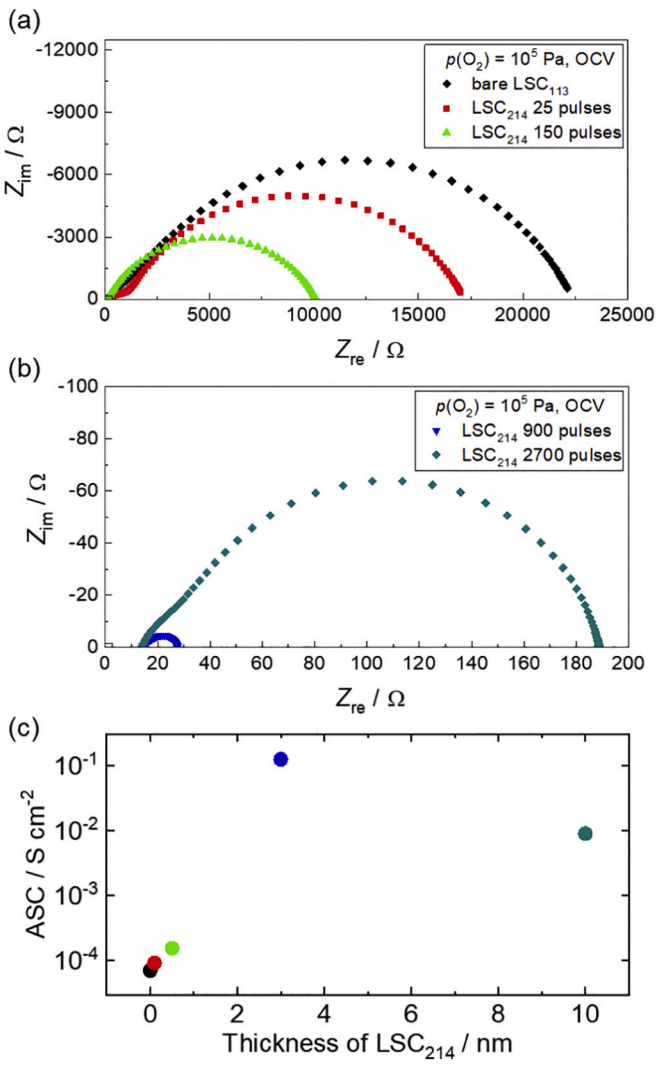

Fig. 2. Nyquist plot from EIS at 1073 K and $p(O_2)$ of 10^5 Pa for (a) bare LSC_{113} and LSC_{214}-decorated LSC_{113} (25 and 150 pulses); (b) LSC_{214}-decorated LSC_{113} (900 and 2700 pulses). (c) Area specific interfacial conductivity as a function of LSC_{214} layer thickness.

3. Results and discussion

The crystal structures of each prepared thin film on a SiO_2 glass substrate were characterized. XRD patterns of GDC (the buffer layer) and LSC_{113} and LSC_{214} thin films on SiO_2 are shown in Fig. S2. All peaks were identified on the basis of the reported crystal structures for GDC, LSC_{113}, and LSC_{214}. The lattice constants of the thin films were consistent with the database (Table S1). We confirmed the formation of an LSC_{113} phase for the LSC_{113} thin film at the (110) YSZ plane, as shown in Fig. S3. AFM analysis demonstrated that LSC_{113} and $LSC_{113/214}$ films at the (110) YSZ plane had a small surface roughness with root-mean-square values of ~1.32 and ~ 3.01 nm, respectively (Fig. S4). The cross-sectional TEM images of the thin films are shown in Fig. S5; dense film layers with thicknesses of 60, 3, and 25 nm were obtained for LSC_{113}, LSC_{214}, and GDC, respectively. These results confirmed that the

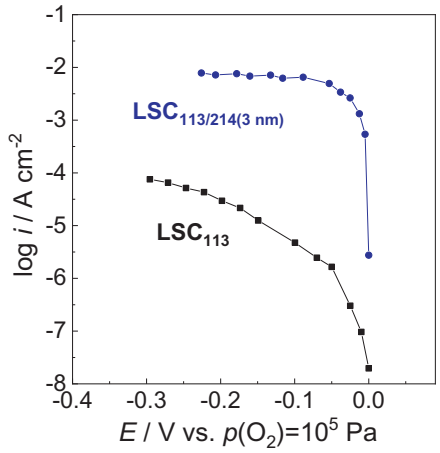

Fig. 3. Current–potential curve for LSC_{113} and $LSC_{113/214}$ on YSZ at 1073 K and $p(O_2)$ of 10^5 Pa.

prepared thin films could be used as model electrodes to investigate their surface phenomena *via operando* TRF-XAS.

Previous studies have reported enhanced ORR kinetics through the decoration of LSC_{113} with LSC_{214} [13,16]. Similarly, in our thin film study, this kinetics enhancement using LSC_{214} decoration was also observed through EIS and DC polarization measurements. Fig. 2 shows Nyquist plots and the calculated area specific conductivity obtained from EIS measured at 1073 K and $p(O_2)$ of 10^5 Pa. It can be observed that LSC_{214} decoration decreased the resistance related to the semicircle up to 3 nm (900 pulses of LSC_{214} deposition) and increased at 10 nm (2700 pulses). This represents an enhancement approximately three orders of magnitude higher for the decoration of 3 nm LSC_{214} compared to that for bare LSC_{113}. However, electrode kinetics slightly decreased to 10 nm for LSC_{214}. The enhanced kinetics could also be confirmed through the DC polarization measurements for the bare LSC_{113} and the LSC_{113} with a 3 nm LSC_{214} deposition, at 1073 K and $p(O_2)$ of 10^5 Pa (Fig. 3). As shown in Fig. 3, the current density for $LSC_{113/214}$ significantly increased. These trends were consistent with those reported in previous studies [13,16]. We will discuss the surface chemistry from the results obtained by TRF-XAS and XRF using the bare LSC_{113} and the 3 nm LSC_{214} decoration on LSC_{113} sample ($LSC_{113/214}$).

Operando Co K-edge XANES of LSC thin films enables us to determine the oxidation state obtained from electrochemical cathodic polarization. In addition, the TRF setup provides surface-sensitive information, which is compared with the bulk information. Fig. 4 shows the normalized Co K-edge XANES spectra for LSC_{113} and $LSC_{113/214}$ under different applied potentials at 773 K and $p(O_2)$ of 10^5 Pa. Bulk information for LSC_{113} and $LSC_{113/214}$ from the standard fluorescence XAS spectra is depicted in Figs. 4a and b, respectively. When cathodic polarization increased, the absorption edge observed at 7720 eV shifted toward the lower energy side. The absorption energy of Co K-edge XANES in LSC corresponded to the oxidation state of cobalt in the electrodes, which was determined by oxygen nonstoichiometry [40]. The low energy shift observed in LSC_{113} and $LSC_{113/214}$ indicated that cathodic polarization induced oxygen vacancy in LSC and decreased the oxygen chemical potential, which will be further discussed quantitatively in the following section. The surface-sensitive XANES spectra for LSC_{113} and $LSC_{113/214}$ from the TRF measurements are illustrated in Figs. 4c and d, respectively. It should be noticed that even at low cathodic polarization, a drastic profile change was induced in the Co K-edge XANES spectra for LSC_{113}, while a continuous energy shift was observed in the bulk XANES data. Compared with the Co K-edge XANES spectra under OCV, the XANES spectra measured at 100 mV broadened and located at lower energy. This structural change is related to the Sr enrichment in the LSC phase

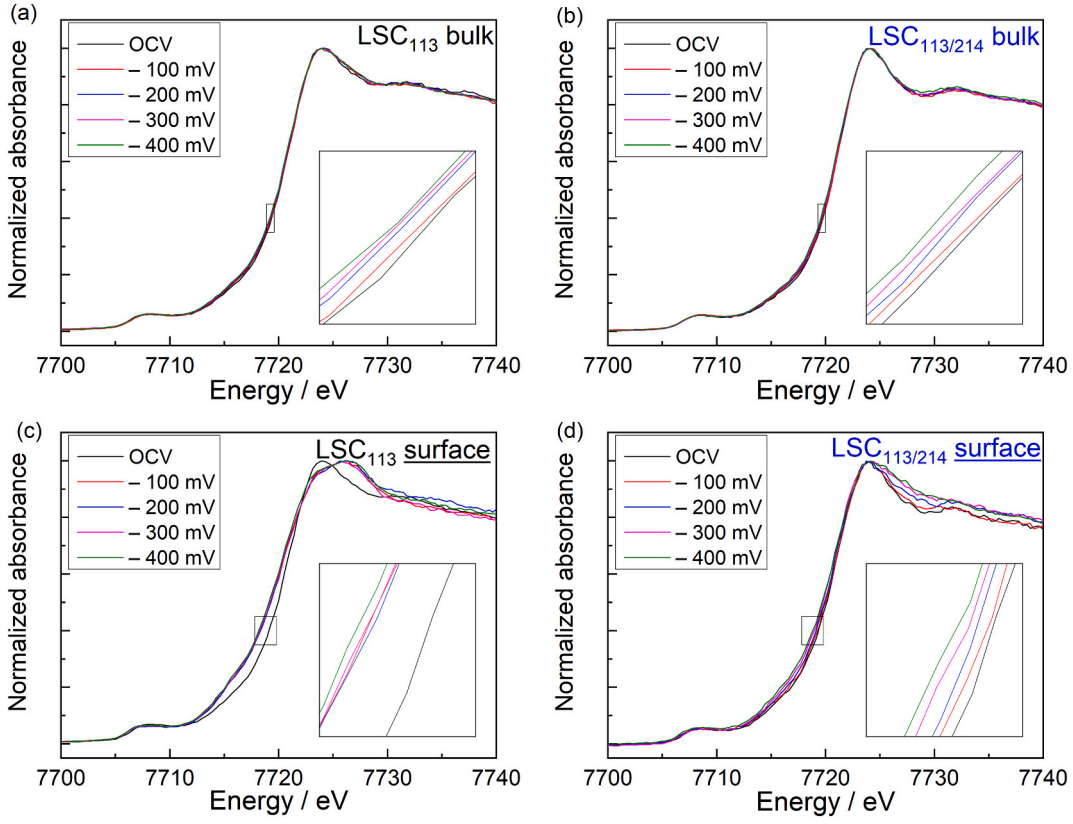

Fig. 4. Co K-edge XANES spectra from *operando* TRF-XAS for (a, c) LSC_{113} and (b, d) $LSC_{113/214}$, measured under cathodic polarization at 773 K and $p(O_2)$ of 10^5 Pa. (a, b) Bulk information from the standard fluorescence XAS and (c, d) surface information under the TRF condition.

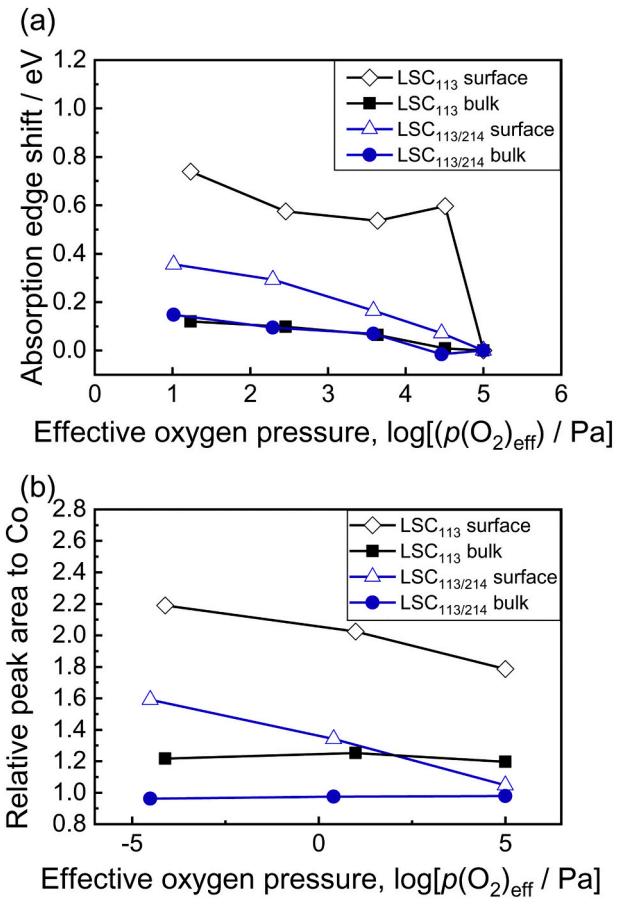

Fig. 5. (a) Absorption edge shift at the Co K-edge as a function of effective oxygen partial pressure for the *operando* TRF-XAS. (b) Relative peak area changes of Sr-K normalized by the peak area of Co-K for the *operando* TRF-XRF. Open squares denote the shift measured under various $p(O_2)$ under OCV. Cross symbols represent the shift measured when applying different DC biases at $p(O_2)$ of 10^5 Pa.

because of the similarity with the corresponding XANES spectra for $Sr_6Co_5O_{15}$, which is a Sr-rich and non-stoichiometric compound [39]. In addition, the XANES spectra for $LSC_{113/214}$ showed a gradual increase in edge inclination, implying that Sr-rich phase formation was suppressed at low cathodic polarization. The surface XANES spectra significantly changed upon potential application. As the bulk XANES spectra showed negligible differences between LSC_{113} and $LSC_{113/214}$ upon potential application, the structural difference is the nanoscale ordered phenomena at the surface, which cannot be explained by conventional techniques in order to analyze bulk materials. The estimated edge energy shift as a function of the applied voltage is provided in Fig. S6 in the supporting information.

The edge energy shift, which is an indicator of the oxidation state, was further analyzed as a function of the effective oxygen partial pressure, $p(O_2)_{eff}$. The electrode polarization potentials, η, were calculated using the following expression:

$$\eta = V_{apply} - R_{bulk} I \quad (1)$$

where V_{apply}, R_{bulk}, and I are the voltage applied to the cell, electrolyte resistance, and current, respectively. Under polarization conditions, $p(O_2)_{eff}$ is defined in terms of η as follows:

$$p(O_2)_{eff} = exp\left\{\frac{2\mu_{O,eff}}{RT}\right\} = p(O_2)exp\left\{\frac{4F\eta}{RT}\right\} \quad (2)$$

where R is the gas constant and F is the Faraday constant. Under OCV, ($\eta = 0$), $p(O_2)_{eff}$ is equivalent to $p(O_2)$. In this study, the application of −400 mV between the two electrodes (WE–CE) corresponded to $p(O_2)_{eff}$ that was approximately four orders of magnitude high. The energy shift calculated from Co K-edge XANES spectra as a function of $p(O_2)_{eff}$ is shown in Fig. 5a. For bulk XANES, there was no difference between the spectral results for LSC_{113} and $LSC_{113/214}$. This demonstrated that the oxygen potential change induced by cathodic polarization is similar for LSC_{113} and $LSC_{113/214}$; thus, these LSC had the same rate-determining step in the reaction mechanism (probably surface reaction limitation as in previously reported studies [4]). The surface oxidation state exhibited an evident difference between LSC_{113} and $LSC_{113/214}$. While the energy shift on the LSC_{113} surface was induced under small polarization, a gradual energy shift was observed for $LSC_{113/214}$. The energy shift for $LSC_{113/214}$ even at $p(O_2)_{eff}$ of 10 Pa was lower than that for LSC_{113} at $p(O_2)_{eff}$ of 10^4 Pa. As mentioned previously, the energy shift was related to Sr enrichment in the LSC phase. The difference in the edge energy shifts confirmed the suppression of that Sr enrichment by LSC_{214} decoration. Previous reports using XPS have not clearly distinguished the surface secondary phase and LSC phases [14,16]. Because the Co K-edge TRF-XAS results directly corresponded to the oxidation state of cobalt oxides, the *operando* XAS results confirmed the Sr enrichment in LSC phases and the suppression effect of LSC_{214} decoration.

To investigate the phenomena related to Sr enrichment in LSC phases, the elemental analysis of for LSC_{113} and $LSC_{113/214}$ was conducted through *operando* TRF-XRF. The XRF spectra are provided in Fig. S7 in the supporting information. The scattered X-ray was observed at 16.5 keV. The peaks observed at approximately 4.5, 6.9, and 14.1 keV can be assigned to La-L, Co-K, and Sr-K, respectively. In addition to these peaks from LSC phases, other fluorescence peaks were detected at 7.9 and 9.1 keV. These peaks can be assigned to Hf-L from the YSZ substrates

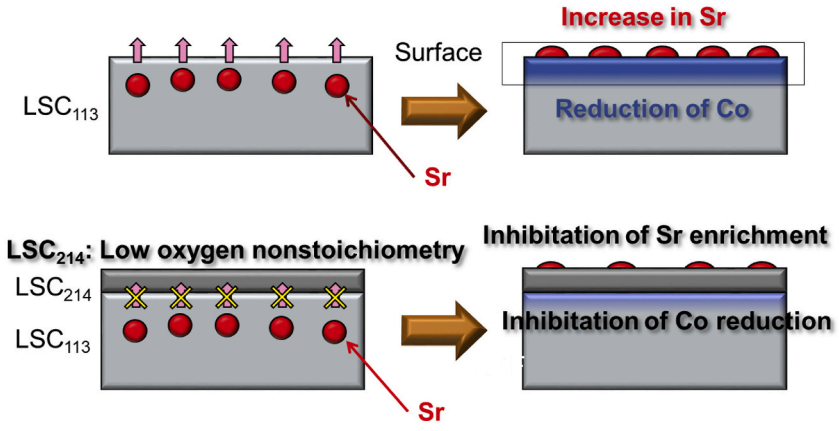

Fig. 6. Schematic of the surface mechanism of LSC_{113} and $LSC_{113/214}$ cathodic polarization at high temperature.

because the YSZ single crystals contain a few weight percent of Hf impurity [41]. Even for the surface-sensitive TRF configuration, the peaks from Hf-L also appeared. This is because the scattered X-ray spreads in all directions, which induces the fluorescence from the substrates. To compare the changes of the relative intensity of Sr fluorescence for LSC_{113} and $LSC_{113/214}$ on the surface and bulk as a function of $p(O_2)_{eff}$, the peak areas of Sr normalized by Co were plotted in Fig. 5b. We note that the higher Sr ratio of LSC_{113} bulk than $LSC_{113/214}$ bulk is within the experimental error. However, compared to the experimental error, we observed a more than twofold change in the area ratio with the bias applied for the surface spectra. While the peak areas of Sr at the surface for LSC_{113} and $LSC_{113/214}$ increased under cathodic polarization, the peaks of the bulk did not change under polarization. For LSC_{113}, the amount of Sr on the surface remarkably increased, which demonstrated Sr enrichment in the LSC phase because XRF detects La and Co simultaneously. Although an increase in Sr fluorescence intensity at the surface was also observed for $LSC_{113/214}$, the amount of enriched Sr significantly decreased, which is also in agreement with the energy shift of *operando* Co K-edge XANES spectra.

The experimental results provided insights into the surface mechanism under cathodic polarization at high temperature, as shown in Fig. 6. Although the *operando* XAS and XRF measurements were performed at 773 K due to the limitation of thermal insulation properties of the cell, the observed phenomena are expected to be also happen at higher temperature condition. The cathodic polarization of LSC_{113} induced the predominant Sr enrichment on the surface, which decreased ORR activity due to deviation from the ideal electronic state, such as the O p-band center [42]. The driving force of Sr enrichment is the high temperature and/or electrochemically derived reducing conditions at the electrode surface. These essential factors cannot be avoided, and the subsequent Sr migration can be disturbed by surface modification of the secondary phase such LSC_{214}. Compared to LSC_{113}, the amount of oxygen nonstoichiometry for LSC_{214} was considerably low [43,44], which hindered the atomic configuration change in the crystal. When the LSC_{214} phase was decorated on the LSC_{113} surface, this inertial property of LSC_{214} prevented Sr from moving toward the surface of LSC_{113}, which preserved the ideal band structure of LSC_{113}.

4. Conclusion

Dense LSC_{113} and $LSC_{113/214}$ thin film electrodes on the YSZ substrate with a GDC interlayer were prepared. From the results, it can be concluded that LSC_{214} decoration on LSC_{113} enhanced ORR activity by more than two orders of magnitude at high temperature. *Operando* TRF-XAS and XRF under cathodic polarization were performed. The predominant surface reduction of Co ions with Sr enrichment under cathodic polarization was observed for LSC_{113}. This was suppressed by LSC_{214} decoration, which improved ORR activity of the as-prepared electrode.

Declaration of Competing Interest

The authors have no conflicts of interest directly relevant to the content of this article.

Acknowledgment

This work was supported by JSPS KAKENHI Grant Number JP25810134 and JP18H03929. The synchrotron radiation experiments were performed at SPring-8 with the approval of the Japan Synchrotron Radiation Research Institute (JASRI).

Appendix A. Supplementary data

Supplementary data to this article can be found online at https://doi.org/10.1016/j.ssi.2020.115502.

References

[1] E.D. Wachsman, K.T. Lee, Lowering the temperature of solid oxide fuel cells, Science 334 (2011) 935–939.
[2] D.J.L. Brett, A. Atkinson, N.P. Brandon, S.J. Skinner, Intermediate temperature solid oxide fuel cells, Chem. Soc. Rev. 37 (2008) 1568–1578.
[3] J. Mizusaki, K. Amano, S. Yamauchi, K. Fueki, Electrode reaction at Pt, O_2(g)/stabilized zirconia interfaces. Part I: Theoretical consideration of reaction model, Solid State Ionics 22 (1987) 313–322.
[4] T. Kawada, J. Suzuki, M. Sase, A. Kaimai, K. Yashiro, Y. Nigara, J. Mizusaki, K. Kawamura, H. Yugami, Determination of oxygen vacancy concentration in a thin film of $La_{0.6}Sr_{0.4}CoO_{3-\delta}$ by an electrochemical method, J. Electrochem. Soc. 149 (2002) E252–E259.
[5] S.B. Adler, Factors governing oxygen reduction in solid oxide fuel cell cathodes, Chem. Rev. 104 (2004) 4791–4843.
[6] Y. Orikasa, T. Ina, K. Yamamoto, T. Nakao, A. Mineshige, K. Amezawa, T. Kawada, H. Tanida, T. Uruga, Y. Uchimoto, Direct observation of rate determining step for Nd_2NiO_{4+d} SOFC cathode reaction by operando electrochemical XAS, Electrochemistry 82 (2014) 897–900.
[7] T. Nakamura, R. Oike, Y. Kimura, Y. Tamenori, T. Kawada, K. Amezawa, Operando soft X-ray absorption spectroscopic study on a solid oxide fuel cell cathode during electrochemical oxygen reduction, Chemsuschem 10 (2017) 2008–2014.
[8] Y. Tsuji, K. Amezawa, T. Nakao, T. Ina, T. Kawada, K. Yamamoto, Y. Uchimoto, Y. Orikasa, Investigation of cathodic reaction mechanism in solid oxide fuel cells by operando X-ray absorption spectroscopy, Electrochemistry Advanced Publication (2020), https://doi.org/10.5796/electrochemistry.20-00108.
[9] K. Amezawa, X-ray absorption spectroscopic studies on solid oxide fuel cells and proton-conducting ceramic fuel cells, Current Opinion in Electrochemistry 21 (2020) 250–256.
[10] Y. Ohno, S. Nagata, H. Sato, Effect of electrode materials on the properties of high-temperature solid electrolyte fuel cells, Solid State Ionics 3-4 (1981) 439–442.
[11] N. Teiji, M. Makoto, Y. Yukio, Reduction-oxidation and catalytic properties of Perovskite-type mixed oxide catalysis ($La_{1-x}Sr_xCoO_3$), Chem. Lett. 10 (1981) 1589–1592.
[12] E.J. Crumlin, E. Mutoro, S.J. Ahn, D.N. Leonard, A. Borisevich, M.D. Biegalski, H. M. Christen, Y. Shao-Horn, Oxygen reduction kinetics enhancement on a heterostructured oxide surface for solid oxide fuel cells, J. Phys. Chem. Lett. 1 (2010) 3149–3155.
[13] E. Mutoro, E.J. Crumlin, M.D. Biegalski, H.M. Christen, Y. Shao-Horn, Enhanced oxygen reduction activity on surface-decorated perovskite thin films for solid oxide fuel cells, Energy Environ. Sci. 4 (2011) 3689–3696.
[14] E.J. Crumlin, E. Mutoro, Z. Liu, M.E. Grass, M.D. Biegalski, Y.-L. Lee, D. Morgan, H. M. Christen, H. Bluhm, Y. Shao-Horn, Surface strontium enrichment on highly active perovskites for oxygen electrocatalysis in solid oxide fuel cells, Energy Environ. Sci. 5 (2012) 6081–6088.
[15] E. Mutoro, E.J. Crumlin, H. Pöpke, B. Luerssen, M. Amati, M.K. Abyaneh, M. D. Biegalski, H.M. Christen, L. Gregoratti, J. Janek, Y. Shao-Horn, Reversible compositional control of oxide surfaces by electrochemical potentials, J. Phys. Chem. Lett. 3 (2012) 40–44.
[16] E.J. Crumlin, E. Mutoro, W.T. Hong, M.D. Biegalski, H.M. Christen, Z. Liu, H. Bluhm, S.H. Yang, In situ ambient pressure X-ray photoelectron spectroscopy of cobalt Perovskite surfaces under cathodic polarization at high temperatures, J. Phys. Chem. C 117 (2013) 16087–16094.
[17] Z. Feng, E.J. Crumlin, W.T. Hong, D. Lee, E. Mutoro, M.D. Biegalski, H. Zhou, H. Bluhm, H.M. Christen, Y. Shao-Horn, In situ studies of the temperature-dependent surface structure and chemistry of single-crystalline (001)-oriented $La_{0.8}Sr_{0.2}CoO_{3-\delta}$ perovskite thin films, J. Phys. Chem. Lett. 4 (2013) 1512–1518.
[18] Z. Feng, Y. Yacoby, M.J. Gadre, Y.-L. Lee, W.T. Hong, H. Zhou, M.D. Biegalski, H. M. Christen, S.B. Adler, D. Morgan, Y. Shao-Horn, Anomalous interface and surface strontium segregation in $(La_{1-y}Sr_y)_2CoO_{4\pm\delta}/La_{1-x}Sr_xCoO_{3-\delta}$ heterostructured thin films, J. Phys. Chem. Lett. 5 (2014) 1027–1034.
[19] E.J. Crumlin, Z. Liu, H. Bluhm, W. Yang, J. Guo, Z. Hussain, X-ray spectroscopy of energy materials under in situ/operando conditions, J. Electron Spectrosc. Relat. Phenom. 200 (2015) 264–273.
[20] W.T. Hong, K.A. Stoerzinger, E.J. Crumlin, E. Mutoro, H. Jeen, H.N. Lee, Y. Shao-Horn, Near-ambient pressure XPS of high-temperature surface chemistry in $Sr_2Co_2O_5$ thin films, Top. Catal. 59 (2016) 574–582.
[21] Y. Yu, A.Y. Nikiforov, T.C. Kaspar, J.C. Woicik, K.F. Ludwig, S. Gopalan, U.B. Pal, S.N. Basu, Chemical characterization of surface precipitates in $La_{0.7}Sr_{0.3}Co_{0.2}Fe_{0.8}O_{3-\delta}$ as cathode material for solid oxide fuel cells, J. Power Sources 333 (2016) 247–253.
[22] M. Rohnke, K. Schaepe, A.K. Bachmann, M. Laenger, J. Janek, In situ ToF-SIMS monitoring of SOFC cathodes – A case study of $La_{0.74}Sr_{0.17}Mn_{1.01}O_{2.9}$ model electrodes, Appl. Surf. Sci. 422 (2017) 817–827.
[23] M. Niania, R. Podor, T.B. Britton, C. Li, S.J. Cooper, N. Svetkov, S. Skinner, J. Kilner, In situ study of strontium segregation in $La_{0.6}Sr_{0.4}Co_{0.2}Fe_{0.8}O_{3-\delta}$ in ambient atmospheres using high-temperature environmental scanning electron microscopy, J. Mater. Chem. A 6 (2018) 14120–14135.
[24] M. Sase, F. Hermes, K. Yashiro, K. Sato, J. Mizusaki, T. Kawada, N. Sakai, H. Yokokawa, Enhancement of oxygen surface exchange at the hetero-interface of $(La,Sr)CoO_3/(La,Sr)_2CoO_4$ with PLD-Layered films, J. Electrochem. Soc. 155 (2008) B793–B797.
[25] M. Sase, K. Yashiro, K. Sato, J. Mizusaki, T. Kawada, N. Sakai, K. Yamaji, T. Horita, H. Yokokawa, Enhancement of oxygen exchange at the hetero interface of (La,Sr)$CoO_3/(La,Sr)_2CoO_4$ in composite ceramics, Solid State Ionics 178 (2008) 1843–1852.

[26] K. Yashiro, T. Nakamura, M. Sase, F. Hermes, K. Sato, T. Kawada, J. Mizusaki, Composite cathode of perovskite-related oxides, (La,Sr)$CoO_{3-\delta}$/(La,Sr)$_2CoO_{4-\delta}$, for solid oxide fuel cells, Electrochem. Solid-State Lett. 12 (2009) B135–B137.
[27] J.W. Han, B. Yildiz, Mechanism for enhanced oxygen reduction kinetics at the (La,Sr)$CoO_{3-\delta}$/(La,Sr)$_2CoO_{4+\delta}$ hetero-interface, Energy Environ. Sci. 5 (2012) 8598–8607.
[28] J. Mizusaki, Y. Mima, S. Yamauchi, K. Fueki, H. Tagawa, Nonstoichiometry of the perovskite-type oxides $La_{1-x}Sr_xCoO_{3-\delta}$, J. Solid State Chem. 80 (1989) 102–111.
[29] K. Amezawa, Y. Orikasa, T. Ina, A. Unemoto, M. Sase, H. Watanabe, T. Fukutsuka, T. Kawada, Y. Terada, Y. Uchimoto, Electronic and local structures of $La_{1-x}Sr_xCoO_{3-\delta}$ studied by in-situ micro XAS measurements, ECS Trans. 13 (2008) 161–164.
[30] A. Hagen, M.L. Traulsen, W.R. Kiebach, B.S. Johansen, Spectroelectrochemical cell for in situ studies of solid oxide fuel cells, J. Synchrotron Rad. 19 (2012) 400–407.
[31] Y. Fujimaki, H. Watanabe, Y. Terada, T. Nakamura, K. Yashiro, S.I. Hashimoto, T. Kawada, K. Amezawa, Direct evaluation of oxygen chemical potential distribution in an SOFC cathode by in situ X-ray absorption spectroscopy, ECS Trans. 57 (2013) (1925-1932).
[32] R.J. Woolley, M.P. Ryan, S.J. Skinner, In situ measurements on solid oxide fuel cell cathodes – simultaneous X-ray absorption and AC impedance spectroscopy on symmetrical cells, Fuel Cells 13 (2013) 1080–1087.
[33] S.Y. Lai, D. Ding, M. Liu, M. Liu, F.M. Alamgir, Operando and in situ X-ray spectroscopies of degradation in $La_{0.6}Sr_{0.4}Co_{0.2}Fe_{0.8}O_{3-\delta}$ thin film cathodes in fuel cells, ChemSusChem 7 (2014) 3078–3087.
[34] B.C. Eigenbrodt, A.M. Young, T.G. Howell, C.U. Segre, T.L. Reitz, High-temperature, in situ X-ray absorption study of Sr_2MgMoO_6 solid-oxide fuel-cell anode materials, ChemElectroChem 2 (2015) 1568–1575.
[35] R. Oike, Y. Okamoto, T. Tokushima, T. Nakamura, K. Amezawa, In-situ simultaneous soft X-ray absorption and emission spectroscopy under controlled atmosphere and temperature, Electrochemistry 84 (2016) 793–796.
[36] D. Takamatsu, Y. Koyama, Y. Orikasa, S. Mori, T. Nakatsutsumi, T. Hirano, H. Tanida, H. Arai, Y. Uchimoto, Z. Ogumi, First in situ observation of the $LiCoO_2$ electrode/electrolyte Interface by Total-reflection X-ray absorption spectroscopy, Angew. Chem. Int. Ed. 51 (2012) 11597–11601.
[37] T. Okumura, T. Nakatsutsumi, T. Ina, Y. Orikasa, H. Arai, T. Fukutsuka, Y. Iriyama, T. Uruga, H. Tanida, Y. Uchimoto, Z. Ogumi, Depth-resolved X-ray absorption spectroscopic study on nanoscale observation of the electrode–solid electrolyte interface for all solid state lithium ion batteries, J. Mater. Chem. 21 (2011) 10051–10060.
[38] D. Takamatsu, T. Nakatsutsumi, S. Mori, Y. Orikasa, M. Mogi, H. Yamashige, K. Sato, T. Fujimoto, Y. Takanashi, H. Murayama, M. Oishi, H. Tanida, T. Uruga, H. Arai, Y. Uchimoto, Z. Ogumi, Nanoscale observation of the electronic and local structures of $LiCoO_2$ thin film electrode by depth-resolved X-ray absorption spectroscopy, J. Phys. Chem. Lett. 2 (2011) 2511–2514.
[39] Y. Orikasa, E.J. Crumlin, S. Sako, K. Amezawa, T. Uruga, M.D. Biegalski, H. M. Christen, Y. Uchimoto, Y. Shao-Horn, Surface strontium segregation of solid oxide fuel cell cathodes proved by in situ depth-resolved X-ray absorption spectroscopy, ECS Electrochemistry Letters 3 (2014) F23–F26.
[40] Y. Orikasa, T. Ina, T. Nakao, A. Mineshige, K. Amezawa, M. Oishi, H. Arai, Z. Ogumi, Y. Uchimoto, X-ray absorption spectroscopic study on $La_{0.6}Sr_{0.4}CoO_{3-\delta}$ cathode materials related with oxygen vacancy formation, J. Phys. Chem. C 115 (2011) 16433–16438.
[41] T. Andersen, K.V. Hansen, M. Mogensen, I. Chorkendorff, Electrochemical removal of segregated silicon dioxide impurities from yttria stabilized zirconia surfaces at elevated temperatures, Solid State Ionics 190 (2011) 60–66.
[42] Y.-L. Lee, J. Kleis, J. Rossmeisl, Y. Shao-Horn, D. Morgan, Prediction of solid oxide fuel cell cathode activity with first-principles descriptors, Energy Environ. Sci. 4 (2011) 3966–3970.
[43] T. Nitadori, M. Muramatsu, M. Misono, Valence control, reactivity of oxygen, and catalytic activity of lanthanum strontium cobalt oxide ($La_{2-x}Sr_xCoO_4$), Chem. Mater. 1 (1989) 215–220.
[44] A. Unemoto, K. Nagao, T. Tairako, K. Amezawa, T. Kawada, Oxygen reduction at the surface and the hetero-Interface of La-Sr-co-O-oxides, ECS Trans. 28 (2010) 59–70.